Nuclear Physics **A402** (1983) 262–274

COULOMB DISPLACEMENT ENERGIES AND DECAY WIDTHS OF ISOBARIC ANALOG STATES FROM Sm(^{3}He, t) at $\theta = 0°$

J. JÄNECKE, F.D. BECCHETTI, W.S. GRAY and R.S. TICKLE

Department of Physics, The University of Michigan, Ann Arbor, Michigan 48109, USA

and

E. SUGARBAKER

Department of Physics, Ohio State University, Columbus, Ohio 43210, USA

Received 1 December 1982
(Revised 19 January 1983)

Abstract: The ^{144,147,148,149,150,152,154}Sm(^{3}He, t)^{144,147,148,149,150,152,154}Eu reactions leading to ground-state isobaric analog states (IAS) have been studied at $\theta = 0°$ and $E(^3\text{He}) = 45.9$ MeV. The Coulomb displacement energies decrease more rapidly than $A^{-1/3}$. Approximately 110 keV of the total decrease of about 470 keV from $A = 144$ (spherical) to $A = 154$ (deformed) can be ascribed to deformation. No discontinuity is apparent at the transition from spherical to deformed shapes at $N = 88 - 90$. This is attributed to two effects: (i) rms radii increase with static deformations *and* with dynamical vibrations; (ii) Coulomb displacement energies depend on rms charge radii *and* on the rms radii of the neutron excess. The data suggest neutron deformations greater than proton deformations for $A = 148$ and 150 but smaller for $A = 152$ and 154. The IAS widths increase from ~ 30 keV to ~ 90 keV and can be attributed to mixing with the $(T_0 - 1)$ component of a proposed isovector giant monopole resonance.

E NUCLEAR REACTIONS ^{144,147,148,149,150,152,154}Sm(^{3}He, t), $E = 45.9$ MeV; measured $\sigma(E_t, \theta = 0°)$. ^{144,147,148,149,150,152,154}Eu deduced IAS, Coulomb displacement energies, deformations, decay widths. Enriched targets, magnetic spectrometer.

1. Introduction

The (^{3}He, t) and (p, n) charge-exchange reactions are well suited to obtain information about isobaric analog states (IAS) of even-A nuclei whereas proton resonance experiments usually yield information for odd-A nuclei (even-A target plus proton). The (^{3}He, t) reaction, especially at 0°, has practical advantages over the alternate (p, n) charge-exchange reaction since the energy resolution is usually much better.

The (^{3}He, t) reaction on the even-A Sm isotopes offers a unique opportunity to study the transition from spherical to deformed nuclear shapes and their influence on Coulomb displacement energies. The transition takes place [1–4]) between $N = 88$ and 90. One might therefore expect a discontinuity if electrostatic energies are

affected by the static deformation of nuclei. Furthermore, since Coulomb displacement energies depend on the distributions of both the proton core and the neutron excess, independent information about these distributions can possibly be deduced. The (^{3}He, t) reaction also permits the determination of IAS decay widths Γ, 0° cross sections and the study of their relationship to other nuclear properties such as the isovector giant monopole resonance.

2. Experimental procedures

A beam of 45.9 MeV $^3He^{++}$ particles from The University of Michigan 83-inch cyclotron, now decommissioned, was used for the measurements. The beam after passing through the targets entered a system of two 180° analyzing magnets set at $\theta = 0°$. The solid angle was $\Delta\Omega = 1.4$ msr. The beam was deflected and stopped in an aluminium baffle located inside the first analyzing magnet. The total beam current was measured by a monitor detector calibrated against the Faraday cup before and after each 0° run. The experimental setup was identical to that used earlier [5]) in a similar study of IAS of the Sn and Te isotopes. Preliminary results for the Sm(^{3}He, t) reactions have been reported previously [6]).

Tritons from the Sm(^{3}He, t) reactions at $\theta = 0°$ have a much higher magnetic rigidity than $^3He^{++}$ particles. They were detected with a position-sensitive solid-state detector located in the focal plane of either the first or a second sequential analyzing magnet. The experimental energy resolution of this system, observed for states with small intrinsic width, was about 40 keV (FWHM) depending on target thickness. This permitted the determination of peak centroids and hence Q-values with high precision. Other details of the measurements including dispersion matching, beam energy determination and calibration via the crossover technique have been reported earlier [5]).

The targets were obtained by evaporating isotopically enriched material (enrichment >95%) onto carbon backings. The target thicknesses $\rho\Delta x$ of 50 to 90 $\mu g/cm^2$ were determined from the energy loss of low energy α-particles and from elastic scattering of 45.9 MeV ^{3}He particles at $\theta_L = \pm 9°$, which is known to be essentially Rutherford scattering. [7]) The uncertainties of the target thicknesses are estimated to be ±15%.

3. Experimental results

Typical position spectra for the ^{144,154}Sm(^{3}He, t) reactions at $\theta = 0°$ to the g.s. IAS in ^{144,154}Eu are shown in fig. 1. They were obtained with the position-sensitive solid-state detectors in the focal plane of the first (figs. 1a, 1b) or the second (fig. 1c) analyzer magnet and they cover ranges of about 530 keV and 270 keV, respectively. The background is low and arises from direct transitions, compound nucleus evaporation to states with lower isospin, and from breakup/pickup reactions

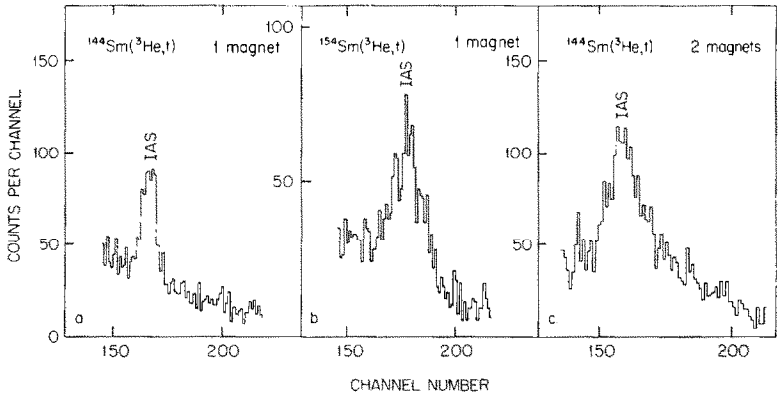

Fig. 1. Spectra of tritons from ^{144,154}Sm(^{3}He, t) to the g.s. IAS in ^{144,154}Eu observed at $\theta = 0°$ and $E(^3\text{He}) = 45.9$ MeV. Spectrum c is obtained with two analyzer magnets and increased dispersion.

such as (^{3}He, tp) [ref. [8])]. The intrinsic widths of the IAS generally exceed the experimental resolution and are described quite well by lorentzian lineshapes. The small asymmetries apparent in the figures result from the non-linear detector response.

There are no indications for strong transitions to other analog states which correspond to states at low excitation energy in the deformed Sm isotopes. This is similar to results for other rare-earth nuclei [9]) and shows the dominance of $l = 0$ transitions at $\theta = 0°$.

TABLE 1

Q-values and Coulomb displacement for Sm (^{3}He, t)

A	$Q(^3\text{He}, t)$ [a]) (keV)	ΔE_C [a]) (keV)	ΔE_C [b]) (keV)	ΔE_C [c]) (keV)
144	−15 311 ± 9	16 075 ± 9		
145			16 002 ± 12	
146				15 950 ± 30
147	−15 125 ± 9	15 889 ± 9		
148	−15 092 ± 9	15 856 ± 9		
149	−15 015 ± 9	15 779 ± 9	15 758 ± 14	
150	−14 984 ± 9	15 748 ± 9		
151			15 712 ± 15	
152	−14 923 ± 9	15 687 ± 9		
153				15 645 ± 30
154	−14 845 ± 9	15 609 ± 9		

[a]) This work; absolute uncertainty ±15 keV.
[b]) From compilation ref. [41]).
[c]) Estimated by interpolating $A^{1/3}\Delta E_C$. No data available for ^{146,153}Sm.

The experimental (^{3}He, t) Q-values are given in table 1. Also included are the Coulomb displacement energies, ΔE_C, deduced from the Q-values using

$$\Delta E_C = -Q(^3\text{He}, \text{t}) + \Delta E_C(^3\text{He}, ^3\text{H}) . \quad (1)$$

Here, $\Delta E_C(^3\text{He}, ^3\text{H}) = 763.8$ keV [ref. [10])] is the Coulomb displacement energy between the mirror nuclei ^{3}He and ^{3}H. The relative and absolute uncertainties in ΔE_C are estimated to be ±9 keV and ±15 keV, respectively. Fig. 2 displays the product of $A^{1/3}$ times ΔE_C as function of A. It indicates that ΔE_C decreases significantly more strongly than $A^{-1/3}$. This appears to be due to the onset of nuclear deformations which leads to increased rms charge radii.

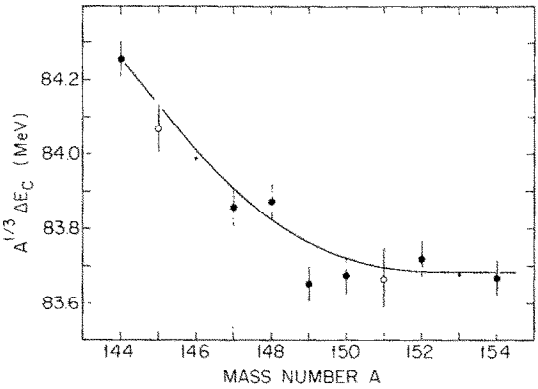

Fig. 2. Coulomb displacement energies times $A^{1/3}$ for the samarium isotopes. Filled circles are from this work. Open circles are from ref. [41]). Estimated values are given as dots. The line is to guide the eye.

The experimental total decay widths Γ of the IAS are listed in table 2. They have been deduced from the observed line shapes by unfolding the experimental resolution. The widths Γ are in the range of 30 keV to 90 keV and generally increase with neutron excess. The spreading widths $\Gamma^{\downarrow}$ were deduced from the experimental widths Γ by applying a small correction (see below). The widths $\Gamma^{\downarrow}$ are displayed in fig. 3 together with theoretical calculations which will also be explained below.

The (^{3}He, t) charge-exchange cross sections at $\theta = 0°$ are displayed in fig. 5. They range from 0.6 to 1.2 mb/sr. As expected [11]) they also generally increase with neutron excess.

4. Discussion

4.1. COULOMB DISPLACEMENT ENERGIES

The emphasis of the present investigation is the study of the dependence of ΔE_C on nuclear shapes. There are several contributions to ΔE_C, but the dominant term,

TABLE 2

Deformed Coulomb displacement energies, deformation parameters, spreading widths and 0° (^{3}He, t) cross sections

A	$\Delta E_C^{def} - \Delta E_C^{sph}$ [a] (keV)	β_2(p) [b]	β_2(n)	$\frac{\beta_2(n)}{\beta_2(p)}$	Γ (keV)	$\Gamma^{\downarrow}$ [c] (keV)	$\frac{d\sigma}{d\Omega}(0°)$ (mb/sr)
144	0±9	0.083±0.009			52±20	52±20	0.61±0.07
145	−35±12 [d]				46±12 [f]	39±12	
146	(−49±30) [e]						
147	−76±9				27±20	20±20	0.79±0.12
148	−68±9	0.136±0.003	0.19±0.04	1.40±0.29	78±20	78±20	1.09±0.14
149	−108±9				102±28 [f] / 61±20	67±16	0.96±0.12
150	−102±9	0.181±0.002	0.24±0.04	1.31±0.22	47±20	47±20	0.99±0.08
151	−102±15 [d]				80±23 [f]	76±23	
152	−91±9	0.279±0.002	0.25±0.03	0.89±0.11	84±20	84±20	1.17±0.17
153	(−92±30 [e])						
154	−97±9	0.308±0.002	0.26±0.03	0.85±0.08	81±20	81±20	1.26±0.13

[a]) Spherical Coulomb displacement energies calculated [9]) from $\Delta E_C^{sph} = aZ_< A^{-1/3} + b$, with a = 1410 keV, and b = −603 keV.

[b]) Refs. [19,20]).

[c]) Spreading widths $\Gamma^{\downarrow}$ calculated from $\Gamma - \Gamma^{\uparrow}$. Here $\Gamma^{\uparrow}$ = 7, ~10, ~4 keV (A = 145, 149, 151) [29]) and $\Gamma^{\uparrow} \approx 7$ keV (A = 147), $\Gamma^{\uparrow} \approx 0$ (A = even) (estimated). (See text.)

[d]) Rev. [41]). [e]) Estimated. [f]) Ref. [29]).

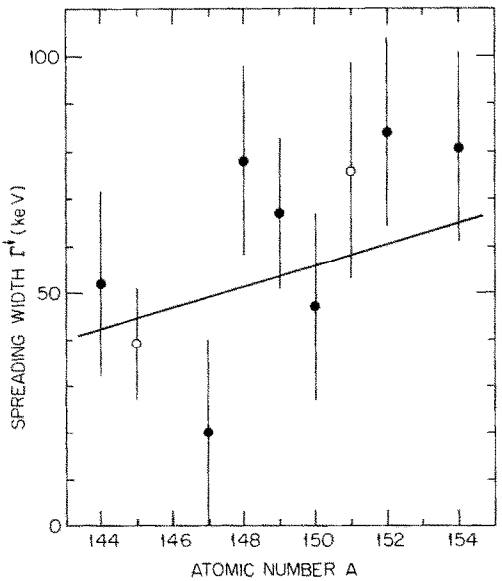

Fig. 3. Spreading width $\Gamma^{\downarrow}$ of the IAS of the Sm isotopes. Filled circles are from this work. The calculated curve is deduced assuming mixing via a charge-dependent Coulomb matrix element V_{CD} with the $(T_0 - 1)$ component of the isovector monopole resonance (eq. (8); see text).

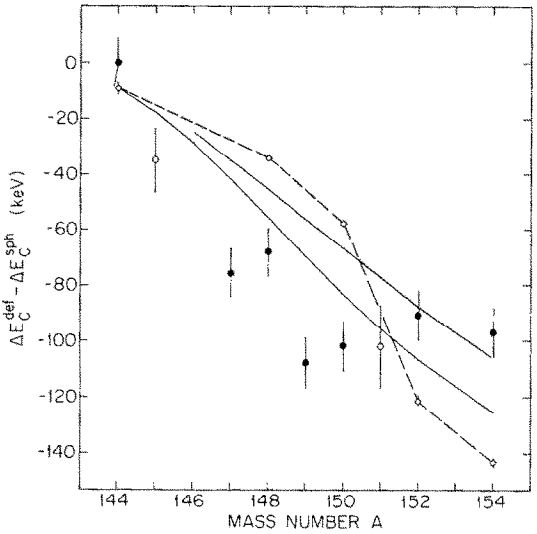

Fig. 4. Coulomb displacement energy differences between deformed and spherical nuclei. The latter are calculated from eq. (3). Data points with filled circles are from this work. The two continuous curves make use of eq. (5) and calculated deformation parameters β_2 and β_4 [ref. [21])]. The upper curve is for $\beta_4 = 0$. The open squares with the dashed curve use experimental parameters β_2 [refs. [19,20])].

well understood for spherical nuclei [12-14]) and contributing about 95%, is the direct Coulomb displacement energy

$$\Delta E_C^{dir} = \frac{1}{2T} \int \rho_{exc}(\boldsymbol{r}) V_{core}(\boldsymbol{r}) \, d^3\boldsymbol{r} . \tag{2}$$

Here, $\rho_{exc}(\boldsymbol{r})$ is the density distribution (including nucleon size) of the neutron excess and $V_{core}(\boldsymbol{r})$ is the Coulomb potential of the proton core. The approach taken in the present work consists of comparing the measured ΔE_C with calculated energies for spherical nuclei and subsequently attempting to interpret the differences in terms of deformed shapes. This procedure is facilitated for the sequence of Sm isotopes by the fact that the g.s. of ^{144}Sm has a spherical shape. The assumption is made that small effects [12]), such as exchange and the electromagnetic spin–orbit interaction, vary smoothly over the sequence of isotopes.

An analytical expression for $\Delta E_C(Z, A)$ for spherical nuclei with diffuse surfaces has been derived [14]). However, the simple two-parameter equation ($Z_< = Z$)

$$\Delta E_C(Z, A) = a \frac{Z_<}{A^{1/3}} + b \tag{3}$$

is also remarkably accurate [13]) and was used in the present analysis. It can be generalized to include the effect of deformed shapes by multiplying the first term

by the factor

$$D(\text{shape}) = 1 - C(\beta_2, \beta_4) = 1 - B_2^2 - \tfrac{4}{21}\sqrt{5}B_2^3 + \tfrac{255}{49}B_2^4 - \tfrac{18}{7}B_2^2B_4 - \tfrac{5}{3}B_4^2, \qquad (4)$$

with $B_2 = \beta_2/(4\pi)^{1/2}$ and $B_4 = \beta_4/(4\pi)^{1/2}$. This expression, derived by Hasse [15]), includes quadrupole and hexadecapole deformation corrections to fourth and second order, respectively. Diffuseness corrections are not included, and the density distributions of proton core and neutron excess are assumed to have equal deformations. Introducing eq. (4) into eq. (3) gives a simple analytical expression for the difference of ΔE_C between deformed and spherical nuclei,

$$\Delta E_C^{\text{def}} - \Delta E_C^{\text{sph}} = -a\frac{Z_<}{A^{1/3}}C(\beta_2, \beta_4). \qquad (5)$$

The energy differences between the experimental and calculated spherical ΔE_C values are included in table 2 and plotted in fig. 4 as a function of A. Eq. (3) is used to describe the spherical ΔE_C. The coefficients $a = 1410$ keV and $b = -603$ keV are from a fit [9]) using eqs. (3) and (4) to *all* available data for $82 < N < 126$. The relative and absolute accuracies of the calculated energies over the range of Sm isotopes are estimated at ±5 keV and ±15 keV, respectively.

The energy differences of fig. 4 display a pronounced and essentially continuous decrease with A from the spherical nucleus ^{144}Sm to the deformed nucleus ^{154}Sm. According to eq. (5), only about 110 keV of the total decrease of about 470 keV is accounted for by changes in the *static* deformation of the Sm ground states. Whereas the quadrupole deformation undergoes a *dis*continuous transition from $\beta_2 \approx 0$ at $A = 150$ to $\beta_2 \approx 0.28$ at $A = 152$, a discontinuity on the order of 100 keV based on a quadratic dependence on β_2 is clearly not apparent in the data of fig. 4.

Part of the explanation for the observed behavior is that Coulomb energies as well as charge radii are affected by both static deformations *and* dynamical vibrations [e.g. refs. [16-18])]. The latter may be viewed microscopically as zero-point motions of collective two-particle/two-hole excitations which give rise to long-range ground-state correlations. Therefore β_2 (and similarly β_4) in eqs. (4) and (5) should be understood to represent the rms values $\langle\beta_2^2\rangle^{1/2}$. Table 2 includes in column 3 values for these quantities deduced from experimental B(E2) values [19,20]). An essentially continuous increase in $\langle\beta_2^2\rangle^{1/2}$ indeed seems to be indicated, and only the values for $A = 152$ and 154 should be interpreted as static deformations.

The two solid curves shown in fig. 4 are calculated using eq. (5) and analytical expressions [21]) for β_2 and β_4 which approximate the deformation parameters of rare-earth nuclei. The general trend of the data is well reproduced provided the nuclear hexadecapole deformation β_4 is included (lower curve; upper curve assumes $\beta_4 = 0$). The effect actually appears to be slightly underpredicted in agreement with ΔE_C data observed for other rare-earth nuclei [9]).

However, if *experimental* values of β_2 (together with calculated or experimental values of β_4) are used with eq. (5) to calculate the effect of deformation on Coulomb

displacement energies, a distinct discrepancy becomes apparent. The dashed curve in fig. 4 connects the values so calculated and is found to significantly underestimate the observed effects for $A = 148$, 150 and to overestimate them for $A = 152,154$. While reflecting a discontinuous component in the A-dependence of β_2, the origin of the discrepancy is believed to be that direct Coulomb displacement energies depend on the distributions of both the proton core *and* the neutron excess. Since this dependence is completely symmetric for the two distributions [16]) the data seem to suggest increased neutron deformations for $A = 148,150$ and reduced neutron deformations for $A = 152,154$. An estimate of the effect can be obtained by replacing the shape-dependent factor of eq. (4) by

$$D(\text{shape}) = (1 - C_1(\beta_2, \beta_4))^{1/2}(1 - C_2(\beta_2, \beta_4))^{1/2}, \tag{6}$$

where the two factors refer to protons and neutron excess, respectively. On the basis of this model, comparison of the data with eqs. (6) and (3) makes it possible to deduce the deformation of the neutron excess from the Coulomb energy data. Using appropriately estimated uncertainties, the ratios $\beta_2(n\text{-exc})/\beta_2(p)$ are found to be on the order of 1.8 ± 0.4 for $A = 148,150$ and 0.6 ± 0.3 for $A = 152,154$. The deformation parameters β_2 for all neutrons were obtained by combining the deformation of the neutron-excess with that of the respective neutron-core (approximated by the proton core). Several averaging procedures were used. The final values are included in table 2. The quoted uncertainties are believed to be realistic as they include realistic estimates of the uncertainties inherent in the various steps of the calculation. As expected from the striking behavior seen in fig. 4, $\beta_2(\text{n})/\beta_2(\text{p}) > 1$ and < 1 for $A = 148,150$ and $A = 152,154$, respectively.

The results displayed in table 2 can be compared to other experimental results which lead to similar conclusions. In a comparison [22]) of proton and neutron elastic and inelastic scattering data on ^{148,152,154}Sm it was found that $\beta_2(\text{n})/\beta_2(\text{p}) \approx 1.18$ for ^{148}Sm but $\beta_2(\text{n})/\beta_2(\text{p}) \approx 1$ (with an estimated uncertainty of several percent) for ^{152,154}Sm. In a comparison [23]) of vector polarized deuteron scattering on ^{152,154}Sm with the corresponding electromagnetic quantities it was found that $\beta_2(\text{n})/\beta_2(\text{p}) \approx 0.85$ to 0.90. While *all* three experimental methods have inherent difficulties, a consistent picture seems to emerge strongly suggesting that the distributions of neutrons and protons have at least slightly different deformations in the transitional ($\beta_2(\text{n})/\beta_2(\text{p}) > 1$) and deformed ($\beta_2(\text{n})/\beta_2(\text{p}) < 1$) Sm isotopes.

4.2. IAS WIDTHS

The total width of an IAS can be expressed as a sum of two components,

$$\Gamma = \Gamma^{\uparrow} + \Gamma^{\downarrow}, \tag{7}$$

where $\Gamma^{\uparrow}$ is the escape width and $\Gamma^{\downarrow}$ the spreading width [24–26]). The escape width is primarily due to T-allowed proton decay (Γ_{p}). The spreading width is due to

mixing with states of lower isospin T_0-1, and its dominant decay mode is neutron decay. The width $\Gamma^{\downarrow}$ would be zero in the absence of Coulomb forces.

The ratio Γ_p/Γ appears to be quite small for even-A nuclei in this mass region. Direct determinations [11,27]) of $\Gamma^{\uparrow} \approx \Gamma_p$ in the Sn region via (p, np) give values of 6 to 24 keV for odd-A nuclei but ≤ 5 keV for neighboring even-A isotopes. This is due to the lower proton decay energies [see also ref. [5])]. No direct determinations of $\Gamma^{\uparrow} \approx \Gamma_p$ appear to exist for even-A rare-earth nuclei, but they have been measured for several odd-A Sm-isotopes [28,29]) and heavier rare-earth nuclei [30]). Values of a few keV are typical, exceeding 10 keV in only a few cases. The width $\Gamma^{\uparrow}$ should again be even smaller for even-A nuclei on account of their lower proton decay energies (by ~ 1.5 MeV). Since the total widths Γ are on the order of 30 to 90 keV, it appears justified to use $\Gamma^{\downarrow} \approx \Gamma$ for $A =$ even and $\Gamma^{\downarrow} \approx \Gamma - 7$ keV for ^{147,149}Sm. These values are included in table 2. Total and spreading widths for three additional odd-A Sm isotopes measured in a proton-resonance experiment [29]) are included in the table.

The spreading widths $\Gamma^{\downarrow}$ of table 2 are displayed in fig. 3. They increase with increasing neutron excess from ~ 30 keV to ~ 90 keV. It is believed that the spreading width originates from mixing via the Coulomb force between the IAS with $T = T_0$ and two types of states of similar internal structure with $T = T_0 - 1$. These are the configuration or anti-analog states and the (T_0-1) component of the isovector monopole resonance (IVM) [25,31,32]). The latter is expected to dominate the mixing in medium-heavy and heavy nuclei. The postulated resonance involves a coherent linear superposition of $J = 0$ coupled neutron–hole/proton–particle states with different radial quantum numbers. The spreading widths are approximately described by [25])

$$\Gamma^{\downarrow} = V_{CD}^2 \frac{\Gamma_{IVM}}{(\Delta E)^2 + (\frac{1}{2}\Gamma_{IVM})^2}, \tag{8}$$

where V_{CD} is the charge-dependent Coulomb matrix element responsible for the mixing with the resonance, and ΔE and Γ_{IVM} are the energy separation from the resonance and the damping width of the resonance, respectively.

The energy difference ΔE between the (T_0-1) component of the isovector monopole resonance and the IAS (or alternately the excitation energy in the target nucleus with $T_z = T_0$) is usually parameterized as [25])

$$\Delta E = E(\mathrm{IVM}_{T_0}) - E_{sym} = \frac{V_{IVM}}{A^{1/3}} - b_{sym}\frac{T_0}{A}. \tag{9}$$

Here, the two terms describe the energy of the T_0 component of the resonance and the energy reduction of the (T_0-1) component which is primarily due to symmetry energy splitting. Several values have been predicted [33,34]) for V_{IVM} and b_{sym}. A recent microscopic theory [35]) applied to four select nuclei from ^{48}Ca to ^{208}Pb is approximately compatible with $V_{IVM} = 155$ MeV and $b_{sym} = 55$ MeV.

Predictions for the excitation energies of the (T_0+1) component of the IVM agree quite well with the energies measured recently for ^{48}Ca, ^{90}Zr and ^{120}Sn via the (π^-, π^0) reaction [36]).

Various estimates have been made for the damping widths Γ_{IVM} of the isovector monopole resonance. Values on the order of 10 MeV seem to be typical [37]), but it is also pointed out that the energy dependence of Γ_{IVM} (strength function) may decrease its value at both higher and lower excitation energies.

The matrix element V_{CD} in eq. (8), finally, can be written as a product of an isospin vector-coupling coefficient and a reduced matrix element. Several simple analytical expressions have been derived for the latter based on hydrodynamical [33]) and microscopic [25,32]) models.

The analysis of the spreading widths $\Gamma^{\downarrow}$ using eq. (8) is difficult because $\Gamma^{\downarrow}$ for an *individual* nucleus is connected with *several* physical quantities, V_{CD}, ΔE and Γ_{IVM}, which all vary with T, A and Z. Only a global analysis of $\Gamma^{\downarrow}$ is therefore likely to yield meaningful results and the use of the simple eq. (8) can only be expected to establish general trends for the parameters of the IVM.

A global analysis for over 50 data points from $A = 112$ to 238 including the $\Gamma^{\downarrow}$ of the Sm isotopes (this work), of the Sn and Te isotopes [5]), and of about 20 recently measured even-A rare-earth nuclei [9]) has been carried out. The strength parameter in V_{CD} and the energies V_{IVM}, b_{sym} and Γ_{IVM} were introduced as adjustable parameters. It became apparent that a dependence on A and/or T had to be introduced for the damping width Γ_{IVM} if ΔE of eq. (9) was calculated with the values $V_{\mathrm{IVM}} = 155$ MeV and $b_{\mathrm{sym}} = 55$ MeV. This was done and very good agreement was obtained. The results for the Sm isotopes are included in fig. 3. The charge-dependent matrix elements appear to be slightly stronger than the calculated values. The damping widths display an increase from about 2 MeV for ^{120}Sn to 4 MeV for ^{208}Pb. Preliminary attempts of a global analysis which included V_{IVM} and b_{sym} as *adjustable* parameters have been reported earlier [38]).

Despite the success in describing the experimental spreading widths $\Gamma^{\downarrow}$ of many medium-heavy and heavy nuclei, the above conclusions must still be considered as tentative.

4.3. CROSS SECTIONS AT 0°

Zero-degree charge-exchange cross sections are included in table 2. They are displayed in fig. 5 and indicate an increase with neutron excess from ~0.6 to ~1.2 mb/sr over the range of targets.

The Lane potential [39]) with its isospin-dependent term has been used successfully to describe cross sections of charge-exchange reactions. Using simple approximations, the cross sections should be approximately proportional to [11,39]) $(N-Z)/A^2$. The dashed curve displayed in fig. 5 is taken from an earlier analysis [5]) of IAS for Sn(^{3}He, t) and Te(^{3}He, t) normalized to ^{118}Sn. The solid curve is a fit to the present

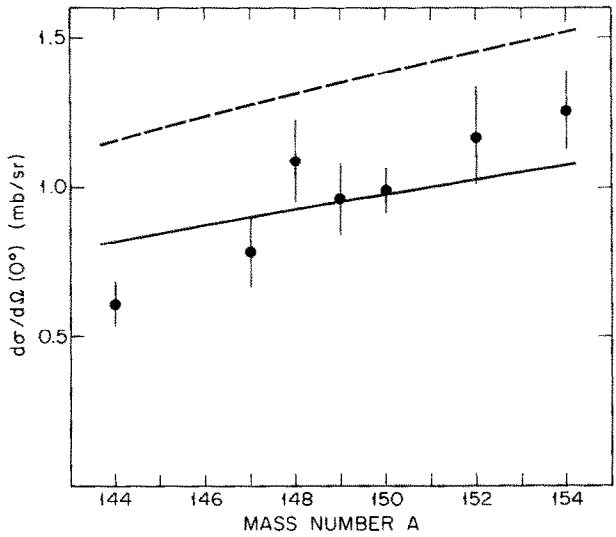

Fig. 5. Cross sections for the (^{3}He, t) charge-exchange reaction at $E(^3\text{He}) = 45.9$ MeV and $\theta = 0°$. The curves correspond to $\sigma = \sigma_0(N-Z)/A^2$ with $\sigma_0 = 850$ mb/sr (solid) and $\sigma_0 = 1200$ mb/sr (dashed). The latter curve is from an analysis of Sn(^{3}He, t) data [5]).

data. While total cross sections often follow a simple dependence on neutron excess [e.g. refs. [11,40])], significant deviations are also observed, [e.g. ref. [5])] particularly for the differential cross sections.

The analysis of the Sn(^{3}He, t) data [5]) using a microscopic $\boldsymbol{t} \cdot \boldsymbol{t}$ interaction yielded an effective interaction of $V_{t\cdot t} = 11 \pm 4$ MeV. This appears to overestimate the data for the spherical and the deformed Sm targets. The fit to the Sm cross sections requires a slightly reduced (~20%) value of $V_{t\cdot t} = 9.3 \pm 3.5$ MeV. These values for $V_{t\cdot t}$ are less than values inferred from other (^{3}He, t) and (p, n) measurements ($V_{t\cdot t} \approx 50$ MeV). However, two-step processes and the filling of Nilsson orbits may affect the interpretation of (^{3}He, t) cross-section data.

5. Summary

The (^{3}He, t) charge-exchange reaction has been studied at $\theta = 0°$ and $E(^3\text{He}) = 45.9$ MeV for the seven stable Sm isotopes. Q-values, and hence Coulomb displacement energies, have been determined. They display effects due to the transitions from spherical to vibrational to statically deformed ground states. The analysis of the data suggests slightly different deformations for the distributions of neutrons and protons, also seen in other experiments [22,23]).

The total widths Γ of the IAS increase with increasing neutron excess from ~30 keV to ~90 keV. It appears that the spreading width $\Gamma^{\downarrow}$, which is due to mixing via the charge-dependent Coulomb interaction with states of lower isospin, is the

dominant contribution to Γ for the even-A isotopes, whereas small but finite contributions from the escape width $\Gamma^{\uparrow}$ have to be included for the odd-A isotopes. A preliminary global analysis of $\Gamma^{\downarrow}$ which assumes mixing with the (T_0-1) component of a proposed isovector giant monopole resonance gives good agreement with the data.

The 0° (^{3}He, t) charge-exchange cross sections increase with increasing neutron excess from ~0.6 to ~1.2 mb/sr. The increase follows approximately a $(N-Z)/A^2$ dependence which is expected from a simple Lane potential or a microscopic $\boldsymbol{t}\cdot\boldsymbol{t}$ interaction.

We thank the cyclotron crew and staff for their assistance. Thanks are due to N. Auerbach, H. Baer, M . Harakeh and K.T. Hecht for useful discussions. This work was supported in part by US National Science Foundation Grant No. 78-07754. The Cyclotron Laboratory was supported by the US Atomic Energy Commission Contract No. AT(11-1)-2167.

References

1) G. Scharff-Goldhaber and J. Weneser, Phys. Rev. **98** (1955) 212
2) J.H. Bjerregaard, O. Hansen, O. Nathan and S. Hinds, Nucl. Phys. **86** (1966) 145
3) P. Debenham and N.M. Hintz, Nucl. Phys. **A195** (1972) 385
4) D.G. Fleming, C. Gunther, G. Hageman, B. Herskind and P.O. Tjom, Phys. Rev. **C8** (1973) 806; W. Oelert, G. Lindstrom and V. Riech, Nucl. Phys. **A233** (1974) 237
5) F.D. Becchetti, W.S. Gray, J. Jänecke, E.R. Sugarbaker and R.S. Tickle, Nucl. Phys. **A271** (1976) 77
6) J. Jänecke, R. Tickle, W.S. Gray, E. Sugarbaker and F.D. Becchetti, Bull. Am. Phys. Soc. **19** (1974) 995
7) D.A. Lewis, A.S. Broad and W.S. Gray, Phys. Rev. C **10** (1974) 2286
8) E.H.L. Aarts, R.K. Bhomik, R.J. de Meijer and S.Y. van der Werf, Phys. Lett. **102B** (1981) 307
9) J. Jänecke, E.H.L. Aarts, A.G. Drentje, M.N. Harakeh and C. Gaarde, Nucl. Phys. **A394** (1983) 39
10) A.H. Wapstra and K. Bos, At. Data and Nucl. Data Tables **19** (1977) 215
11) P.S. Miller and G.T. Garvey, Nucl. Phys. **A163** (1971) 65
12) J.A. Nolen and J.P. Schiffer, Ann. Rev. Nucl. Sci. **19** (1969) 471
13) J. Jänecke, in Isospin in nuclear physics, ed. D.H. Wilkinson (North-Holland, Amsterdam, 1969) ch. 8
14) J. Jänecke, Nucl. Phys. **A181** (1972) 49
15) R.W. Hasse, Ann. Phys. **68** (1971) 377
16) J. Jänecke, in Atomic masses and fundamental constants 4, ed. J. H. Sanders and A. H. Wapstra (Plenum, London, 1972) p. 221
17) S. Ullrich and E.W. Otten, Nucl. Phys. **A248** (1975) 173
18) P.G. Reinhard and D. Drechsel, Z. Phys. **A290** (1979) 85
19) P.H. Stelson and L. Grodzins, Nucl. Data Tables **A1** (1965) 21;
S. Raman, W.T. Milner, C.W. Nestor and P.H. Stelson, Proc. Int. Conf. on nuclear structure (Tokyo, 1977) p. 79
20) K.E.G. Löbner, M. Vetter and V. Hönig, Nucl. Data Tables **A7** (1970) 495
21) J. Jänecke, Phys. Lett. **B103** (1981) 1
22) Ch. Lagrange J. Lachkar, G. Haout, R.E. Shamu and M.T. McEllistrem, Nucl. Phys. **A345** (1980) 193.

23) H. Clement, R. Frick, G. Graw, F. Merz, H.J. Scheerer, P. Schiemenz, N. Seichert and Sun Tsu Ssun, Phys. Rev. Lett. **16** (1982) 1082.
24) A.M. Lane, in Isospin in nuclear physics, ed. D.H. Wilkinson (North-Holland, Amsterdam, 1969) ch. 11
25) N. Auerbach, J. Hüfner, A.K. Kerman and C.M. Shakin, Rev. Mod. Phys. **44** (1972) 48
26) S.Y. van der Werf, N. Blasi, S. Brandenburg, A.G. Drentje, M.N. Harakeh, W.A. Sterrenburg, B. Vischer, A. van der Woude, R. De Leo and H. Janszen, Phys. Lett. **105B** (1981) 111
27) C.A. Whitten, J. Chai, N. Chirapatpimol, W.H. Dunlop and G. Igo, Phys. Lett. **51B** (1974) 45
28) G. Bassani, Y. Cassagnon, C. Levi and R. Papineau, Phys. Lett. **21** (1966) 442
29) R.K. Jolly and C.F. Moore, Phys. Rev. **155** (1967) 1377
30) N.H. Merrill, S.W. Whineray, W.M. Zuk, D.C. Weisser, C.L. Hollas and M. Borsaru, Nucl. Phys. **A216** (1973) 61
31) A.Z. Mekjian, Nucl. Phys. **A146** (1970) 288;
H.A. Weidenmüller, Nucl. Phys. **A99** (1967)
32) N. Auerbach, Nucl. Phys. **A182** (1972) 247
33) A. Bohr, J. Damgaard and B.R. Mottelson, Nuclear structure, ed. A. Hossain *et al.* (North-Holland, 1967) p. 1
34) N. Auerbach and A. Yeverechyahu, Nucl. Phys. **A332** (1979) 173
35) N. Auerbach and A. Klein, Tel-Aviv University Report TAUP 1018–82 and Phys. Rev., to be published
36) H.W. Baer and J.D. Bowman, Int. Conf. on nuclear physics (Amsterdam, 1982);
H. Baer, private communication
37) G.F. Bertsch and S.F. Tsai, Phys. Reports **18C** (1975) 126;
K.F. Liu and G.E. Brown, Nucl. Phys. **A265** (1976) 385;
N. Auerbach and Nguyen Van Giai, Phys. Lett. **72** (1978) 289;
N. Auerbach, V. Bernard and Nguyen Van Giai, Nucl. Phys. **A337** (1980) 143
38) J. Jänecke and M.N. Harakeh, Bull. Am. Phys. Soc. **27** (1982) 704
39) A.M. Lane, Phys. Rev. Lett. **8** (1962) 171; Nucl. Phys. **35** (1962) 676
40) T. Murakami, S. Nashahara, T. Nakagawa, S. Morita, H. Orihara, K. Maeda and K. Miura, Nucl. Phys. **A377** (1982) 163
41) W.J. Courtney and J.D. Fox, At. Data and Nucl. Data Tables **15** (1975) 141